

Review

# Improving the Usage Properties of Steel Using Cold Spray Deposition: A Review

Fabian Cezar Lupu<sup>1</sup>, Corneliu Munteanu<sup>1,2,\*</sup> , Adrian Constantin Sachelarie<sup>1,\*</sup>, Vlad Nicolae Arsenoia<sup>3</sup> and Bogdan Istrate<sup>1,\*</sup> 

- <sup>1</sup> Mechanical Engineering, Mechatronics and Robotics Department, “Gheorghe Asachi” Technical University of Iasi, 700050 Iasi, Romania
- <sup>2</sup> Technical Sciences Academy of Romania, 26 Dacia Blvd., 030167 Bucharest, Romania
- <sup>3</sup> Department of Pedotechnics, Faculty of Agriculture Iasi, University of Life Sciences, 700490 Iasi, Romania
- \* Correspondence: corneliu.munteanu@academic.tuiasi.ro (C.M.); adrian-constantin.sachelarie@academic.tuiasi.ro (A.C.S.); bogdan\_istrate1@yahoo.com (B.I.)

**Abstract:** In this paper, the improvement of the characteristics of different steels that are subjected to extreme operating conditions, including the steels used in the manufacture of various military components, the AISI 52100, the manufacture of bearings, and other types of parts that are also subjected to severe operating conditions were analyzed regarding cold spraying, which uses different types of powders to increase the performance of the materials. The cold, thermal spraying technology “Cold Spray” is a method of processing particles in a solid state. Thermal spraying, based on the dynamic increase in gas acceleration up to supersonic speeds, leads to the obtainment of high kinetic energies, and the accelerated particles are deposited at values that are below their melting point. Research conducted through cold spray technology has seen a significant improvement in material properties; when processing the particles in a solid state, they adhere to the surface instead of eroding it. Cold spraying has proven to be an effective technique for improving material properties, as confirmed by its integration into different fields and industries, becoming competitive by being the only method for depositing particles below their melting point.

**Keywords:** cold spray; microstructure; mechanical properties; corrosion resistance



**Citation:** Lupu, F.C.; Munteanu, C.; Sachelarie, A.C.; Arsenoia, V.N.; Istrate, B. Improving the Usage Properties of Steel Using Cold Spray Deposition: A Review. *Crystals* **2023**, *13*, 245. <https://doi.org/10.3390/cryst13020245>

Academic Editor: José L. García

Received: 30 December 2022

Revised: 20 January 2023

Accepted: 24 January 2023

Published: 31 January 2023



**Copyright:** © 2023 by the authors. Licensee MDPI, Basel, Switzerland. This article is an open access article distributed under the terms and conditions of the Creative Commons Attribution (CC BY) license (<https://creativecommons.org/licenses/by/4.0/>).

## 1. Introduction

The interest given to the improvement of the properties of materials through modern spraying methods, from which numerous pieces of research have been carried out, is reflected in the technological progress that has been made, presenting a continuous development of both the spraying installations and the powders used. At the same time, the desire to contribute to scientific progress through this work has exposed the potential of using surface spraying methods, such as cold spraying, on different types of materials that are subject to severe operating conditions, including the AISI 52100 steel used in the manufacture of bearings, ball screws, etc., as well as the various materials used in the military sector, where, for example, in the case of the manufacture of armor, most are made of homogeneous plates of laminated steel. These are strengthened by the heat treatments of quenching and tempering, which leads to obtaining a hardness of 28–35 HRC [1]. Concerns in this area are derived from mechanical performance deficiencies (and more) and opting for thermal spraying is an increasingly common alternative for redepositing and improving material characteristics. In an article, Champagne claims that this spraying technology (cold spraying) is revolutionary due to the fact that the improvement of the powders has led to the spraying of materials for which it is impossible to give heat treatment.

This technology has proven to be quite effective in the technological processes of repairing various components, as confirmed by the continuous development of both the spraying technology and the powders used in this process [2].

The cold spray approach enables low porosity coatings while retaining the feedstock powder's phase composition. In contrast to thermally sprayed coatings, oxide formation and thermal stresses in the cold sprayed coatings are reduced or entirely eliminated since the working gas temperature during CS is always lower than the melting point of the sprayed material [3]. Thermal spraying is a cost-effective technique for creating thick coatings that may cover any surface and can be created utilizing a greater variety of feedstock materials. Complete or partial melting of the feedstock materials is required for thermal spray technologies, like flame spraying, high-velocity oxy-fuel spraying, and plasma spraying. This can lead to high residual stress in the coatings and material oxidation when the spraying process is carried out in an ambient atmosphere [4,5]. Through this method, the feedstock powder microstructures and characteristics are preserved, preventing oxide formation and other unfavorable structural changes, and improving the longevity of the coatings. Due to the plastic deformation brought on during deposition, cold-sprayed materials have harder surfaces than their equivalent powders and bulk alloys [6].

## 2. Studies Using the Cold Spray Method

When using the cold spray technique, thanks to its many benefits, a variety of industrial items, including turbine blades, pistons, cylinders, bearing components, and shafts, may be produced and repaired. Different coatings can contribute to the features, including hardness, wear and corrosion resistance, and heat conductivity [7].

Trials show that the cold spraying of W is rather ambitious due to the metal's hardness and brittleness at very high temperatures. In contrast, cold spraying can create thick and very dense tantalum (Ta) coatings, which are already used in the space, chemical, and nuclear industries, as well as in medical applications. Metallographic cross-sections of the coatings created by the separate feeding of coarse W and Ta, where 2 mm-thick coatings were produced from the powder, are shown in the microscopic photographs in Figure 1. All of the coatings exhibit little porosity and a growing W volume fraction with an increasing W powder percent, as can be seen from the images [8,9].

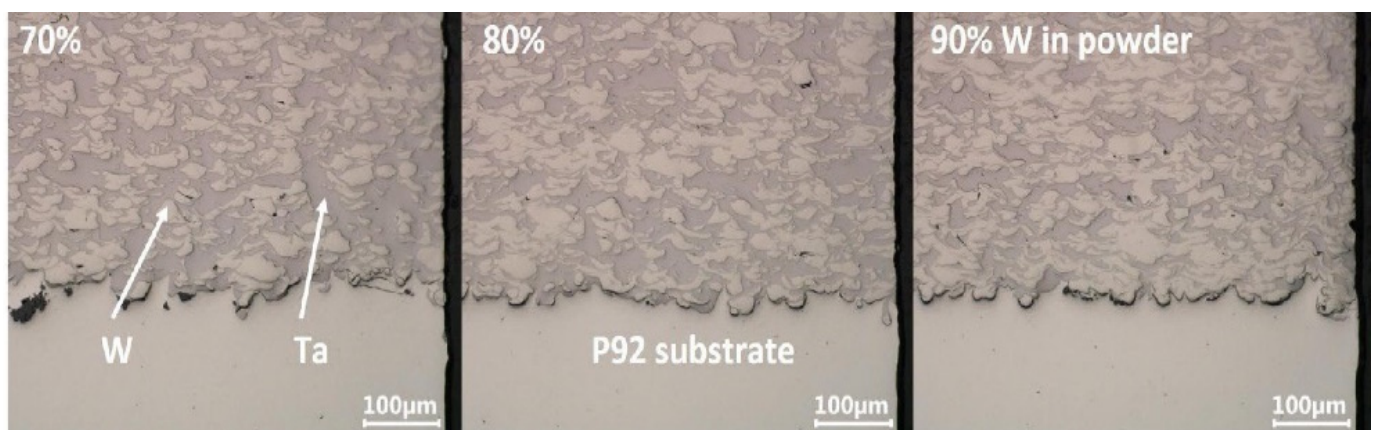


**Figure 1.** Cold spray coatings with varying amounts of tungsten and tantalum, as seen in metallographic cross-sections [8].

The feedstock powder and the high gas consumption rate are the two main cost factors in cold spray technology. Helium has the advantages of efficiency and a high-quality microstructure, but it is also costly. However, nitrogen, the most often researched cold spray propellant gas, is quite affordable [10].

### 2.1. Types of Materials Used for Cold Spray

Of the many types of materials available, for example, ARMOX ballistic plates are produced by metallurgy based on iron ore and through blast furnaces, deoxidized steel in an LD converter and with vacuum treatment results in very clean steel. Through high-tech rolling mills, a fine-grained microstructure is obtained and finally, to obtain the desired hardness/strength properties, the steel is subjected to various specific heat treatments [11,12].

ARMOX plates can be found in a range of hardnesses from homogeneous rolled steel, with a hardness of 280 BHN, to UHH steel, with a hardness of more than 640 BHN, and these are mainly used together with materials such as steel, aluminum, composite materials, etc. [11]. The chemical compositions are presented in Table 1, and the mechanical properties are presented in Table 2 for several types of plates, namely Armox 500 T, Armox 600 T, and Armox Advance [13].

**Table 1.** Chemical composition of ARMOX plate [11].

Name	C Max(%)	Si Max (%)	Mn Max (%)	P Max (%)	S Max (%)	Cr Max (%)	Ni Max (%)	Mo Max (%)	B Max (%)
Armox 500 T	0.32	0.40	1.20	0.010	0.003	1.0	1.80	0.70	0.005
Armox 600 T	0.47	0.70	1.0	0.010	0.003	1.5	3.0	0.70	0.005
Armox advance	0.47	0.70	1.0	0.010	0.003	1.5	3.0	0.7	0.005

**Table 2.** Mechanical properties of ARMOX plate [12].

Name	Hardness (BHN)	0.2% Yield Strength (N/mm <sup>2</sup> )	Tensile Strength (N/mm <sup>2</sup> )	Elongation (%)
Armox 500 T	480–540	min 1250	1450–1750	Min 8
Armox 600 T	570–640	1500	2000	7
Armox advance	HRC58-63	1600	2250	9

Poplawski et al. investigated the fracture properties of Armox 500 T steel with respect to perforation problems through an experimental, numerical procedure to develop the fracture surface in triaxiality and Lode parameter space. The tests performed (including FEM tests, in addition to the practical ones) on several types of samples using three types of punches (pointed, flat, and hemispherical), perforating 1 mm plates, show a sensitivity regarding the Lode parameter, such that the fracture properties depend on this parameter. The greatest force required for perforation was exerted on the hemispherical punch, then the flat one, followed by the pointed one. By means of a Kedzierski model, the highest force obtained was intensified to be between the results of Skoglund's and Iqbal's fracture models. The perforated plates are shown in Figure 2 [14].

In Figure 3 [14], the first trial of the experiment is represented with a solid gray line, a dotted line for the second trial of the experiment, as well as a double-dotted line for the third trial of the experiment, with a solid yellow line for the FEM analysis of the present study, a solid blue line for the FEM analysis of the Skoglund model, a solid green line for the FEM analysis of the Iqbal model, and a solid red line for the FEM analysis of the Kedzierski model.

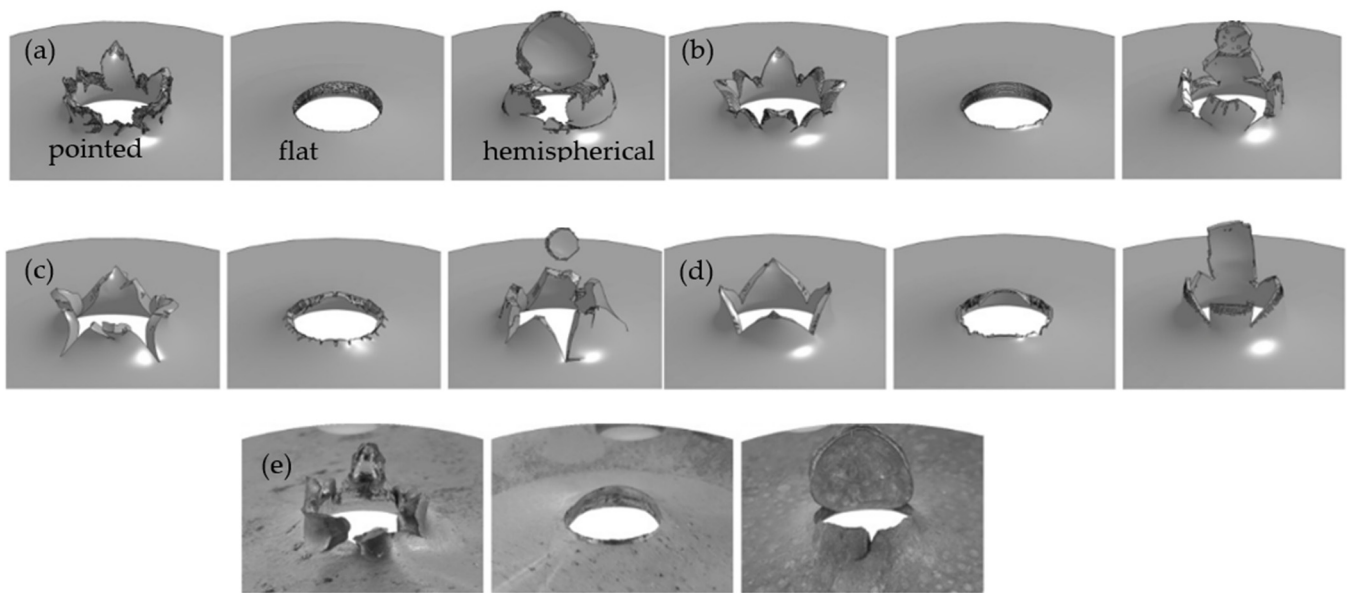


**Figure 2.** (a) FEM present study; (b) FEM Kedzierski; (c) FEM iqbal; (d) FEM Skoglund; (e) Experiment [14].

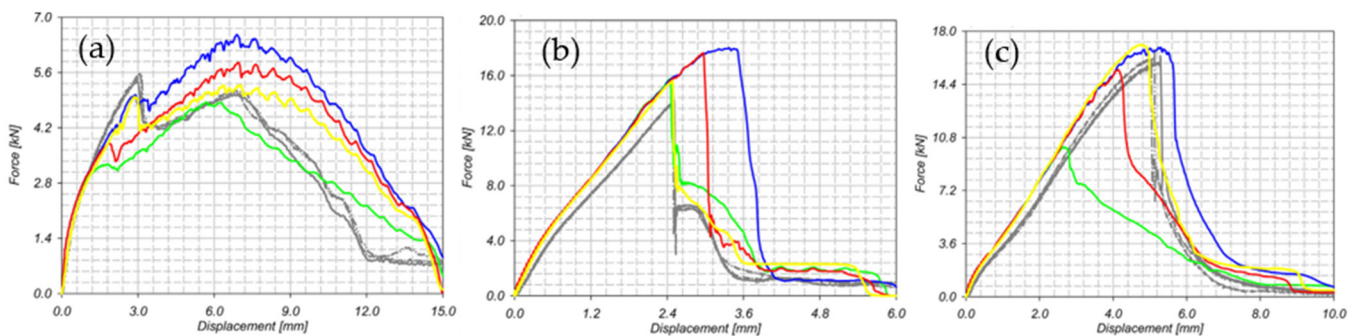


**Figure 3.** Measured plate punching forces: (a) sharp punch, (b) flat punch, and (c) hemispherical punch [14].

## 2.2. Cold Spray Method

Like many materials with high properties, 52100 steel, for example, is distinguished by mechanical properties with respect to elastic stiffness. It has a modulus of elasticity that manages to present high values, namely 210 GPa, leading to the formation of a resistant material while, at the same time, responding well when subjected to processing processes. It also exhibits important properties regarding compressive strength; for example, despite being almost twice as hard as most aluminum alloys, it has a bulk modulus value of 160 GPa. Both the physical and mechanical properties of this type of steel give it properties that make it an excellent material for making parts that must withstand extreme pressures, such as ball screws, aviation bearings, and so on [15,16].

For a better understanding, Kiranbabu et al. approached the mechanism of carbide decomposition in steel 52100 (100Cr6), a mechanism that is crucial for obtaining corrosion-resistant steels that are encountered in industrial applications. The decomposition of cementite is investigated through a modified thermal treatment in order to generate a soft, annealed microstructure in which spherical cementite and lamellar cementite precipitate. In order to investigate the effects of the composition, morphology, and size, as well as the microstructure of the matrix in order to decompose the cementite, the microstructure was subjected to a severe plastic deformation induced by HPT ( $p = 7.56$  GPa,  $Y_{max} \sim 50$ ). After the investigations, it was concluded that adding Cr and Mg leads to an increase in the stability of cementite. Regarding the wear of the spherical cementite precipitates, no wear was observed, with the pearlitic matrix presenting a hardness of 4.7 GPa (in view

of the wear behavior, the decisive role is the hardness of the matrix around the precipitates). In Figure 4, the Y~50 lamella is shown, whereas Figure 4a represents the deformed spherical cementite, and Figure 4b shows the precipitate of the deformed spherical cementite from Figure 4a. A precipitate smaller than (~100 nm) does not indicate any internal deformation [17,18].

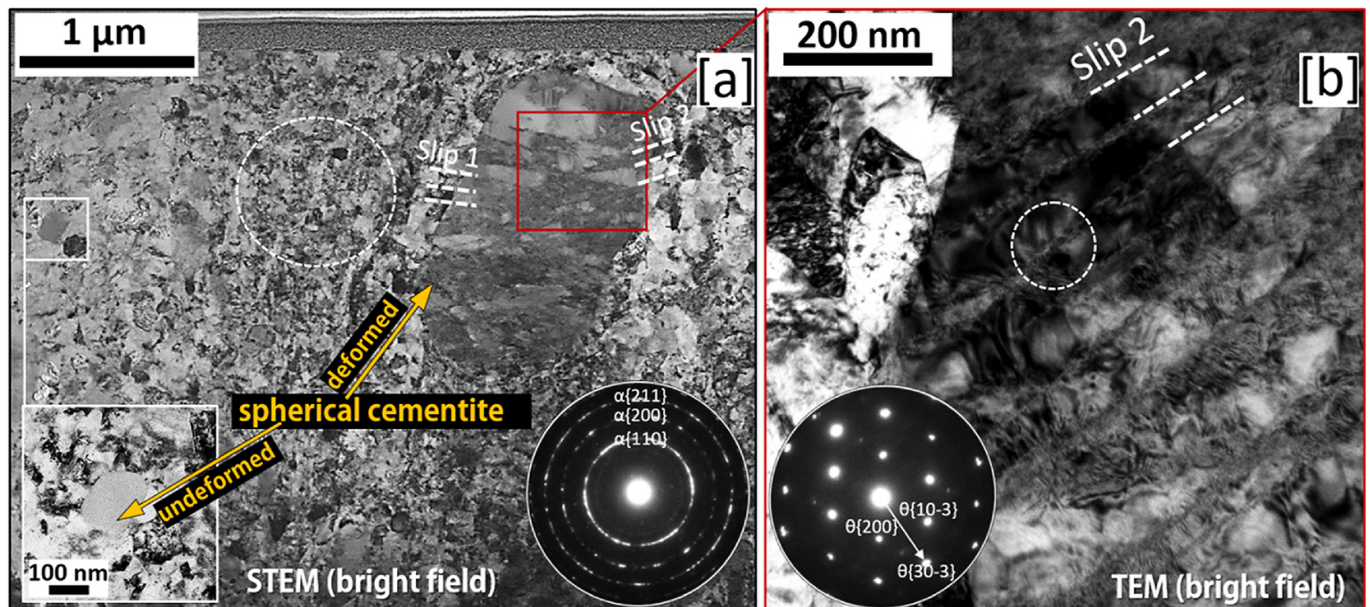


**Figure 4.** TEM image with diffraction analysis of sample Y~50. (a) deformed spherical cementite; (b) precipitate of deformed spherical cementite [17].

In research conducted by Rahbar et al., a 52100-steel substrate using WC-12%Co that was thermally sprayed before friction stir processing (FSP) was carried out on this layer. Before and after FSP, the wear resistance and hardness were tested. FSP combines the sprayed layer with the substrate and lowers porosity and improves hardness and wear performances, according to optical and SEM analysis. Three various structures of the as-sprayed layer are shown in Figure 5a; the WC-12%Co layer is the top porous layer; for improved adhesion, the intermediate layer is a Ni-Al composite, and the bottom layer is the base metal. According to Figure 5b, the refined zone, which contains martensite and WC particles, extends to about 1.2 mm below the surface of the sprayed layer following FSP. The WC is dispersed in a martensitic matrix in this image. When comparing the FSPed structure to the as-sprayed structure, neither the layer boundaries nor the porosity are clearly defined. Since a totally dense microstructure was created by the thermo-mechanical deformation, FSP has solved two drawbacks of sprayed layer: porosity and poor adhesion. The WC particle size is shown in Figure 5c,d, respectively, before and after the FSP. It is obvious that the FSP treatment may reduce the original WC particles to submicron size, and this will affect the hardness and wear performance. During FSP, the smaller WC particles may also experience plastic flow in a Co binder at high temperatures, which would promote a completely thick microstructure and improve WC particle spreading. This would provide a high microhardness [19].

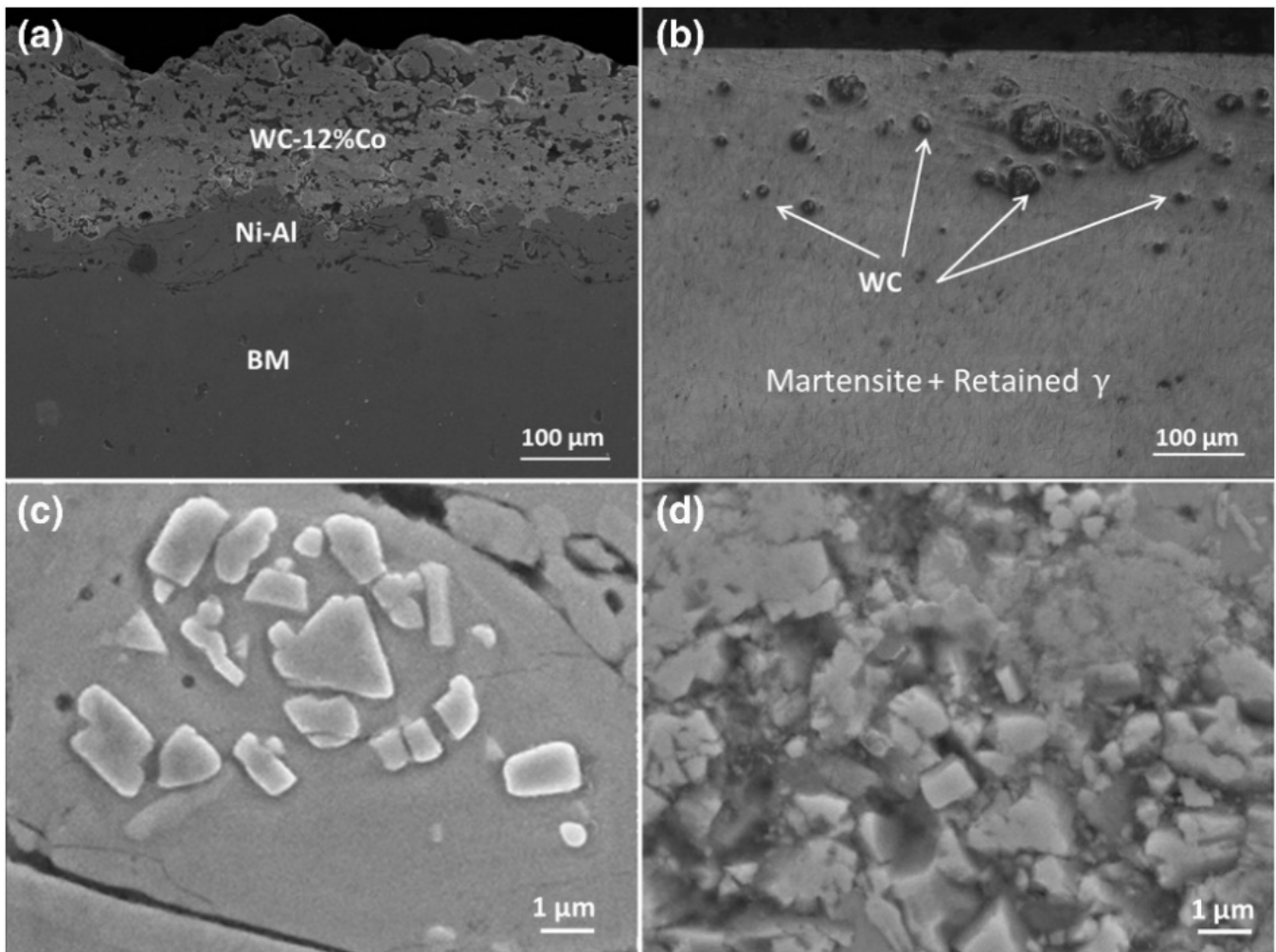


**Figure 5.** The WC particle size (c) before and (d) after FSP, as well as the structure of the sprayed layer (a) before and (b) after FSP [19].

In research conducted by Agiwal et al., in which they repaired the cracks in a 304 L austenitic stainless steel in the field, two methods were investigated: cold spray deposition (CSD) and friction surfacing (FS). Both of these solid-state, low-heat-input methods avoid the negative impacts of solidification, such as compositionally segregated microstructures and shrinkage stresses. Cross-sectional pictures of the coating/substrate contacts fixed by the two procedures are shown in Figure 6. In the steady-state zone, friction surfacing with the consumable rod generated coatings that were 325  $\mu\text{m}$  thick and 2.3 mm broad. The absence of porosity in the coatings and the smooth interface between the coating and substrate point to a strong connection. Figure 6c demonstrates how the FS procedure may patch a fictitious crack. At a depth of 75  $\mu\text{m}$  below the coating/substrate contact, the fracture point was seen to bow. High compressive residual stresses at the surface caused by friction surfacing are thought to have contributed to the substrate's plastic deformation and fracture bending and closing. A high-density cold spray coating (porosity level of less than 0.3%) is seen covering the through-crack in Figure 6b. The coating had a  $\sim 620$   $\mu\text{m}$  thickness. As it got closer to the coating/substrate contact, the crack's breadth shrank. At a distance of approximately  $\sim 90$   $\mu\text{m}$  above the coating/substrate contact, the hairline fracture ultimately vanished. As seen in Figure 6d, some severely damaged powder particles were discovered inside the through-crack. Two potential processes for repairing cracks include compressive stress from the CSD process and the deformation of the substrate at the fracture opening, followed by the application of a stainless-steel coating. For example, the substrate may become smaller as a result of the lateral displacement it experiences as

a result of the powder particles striking it at the crack opening. Due to peening action, complete coverage of the coating may be accomplished during the succeeding particle impact once the crack-opening size is less than the powder particle size ( $<44\ \mu\text{m}$ ). Phase preservation and the lack of deformation-induced martensite distinguish the cold spray coatings from the friction-surfaced coatings [20,21].

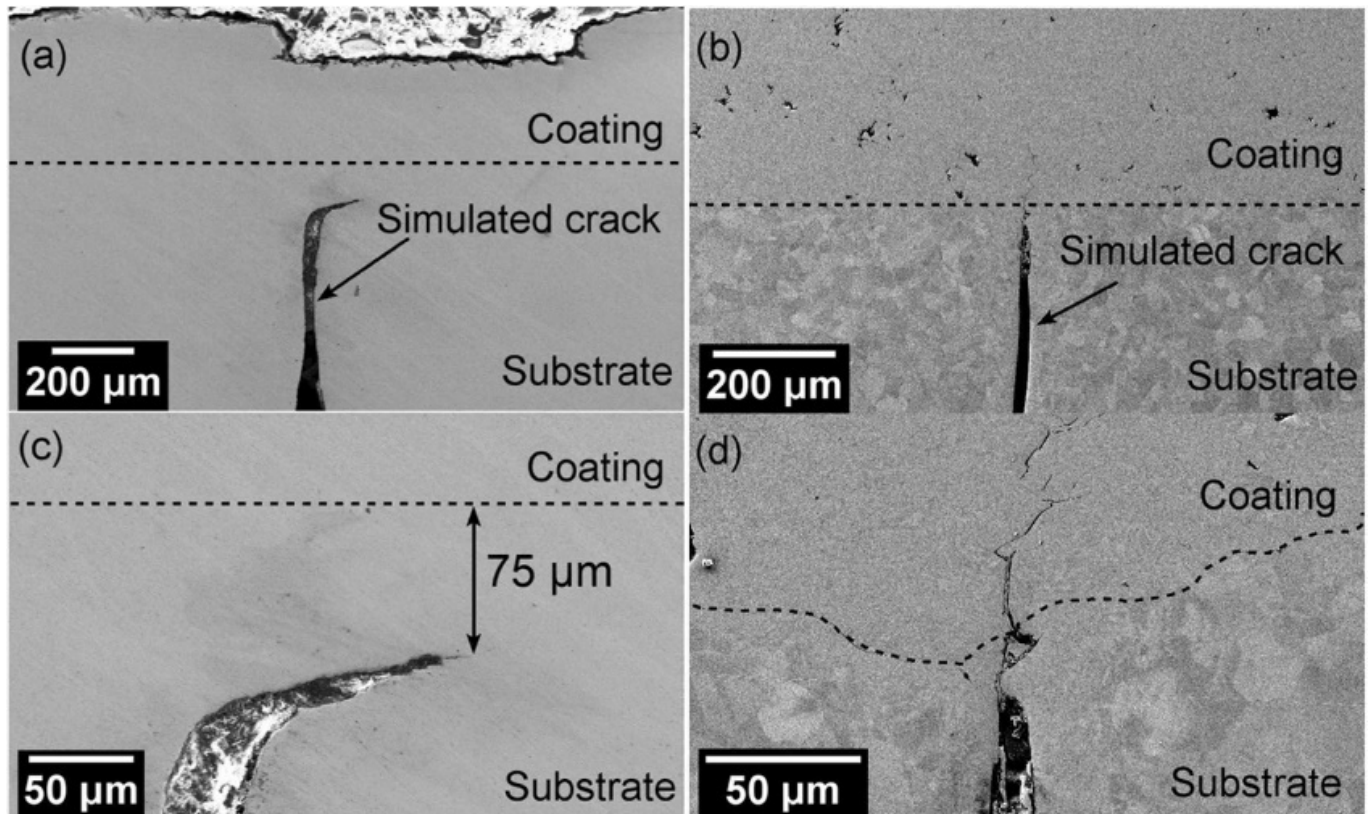


**Figure 6.** SEM cross-sectional pictures of areas that were restored using cold spray deposition (b,d) and friction surfacing (a,c) [20].

Wenpeng et al. carried out a study due to the requirements of the spray gun to be able to facilitate the control of the spray for a long time; these requirements were found due to the studies that attest to the fact that the spray injector (the component that is part of the gun assembly) leads to a disturbance in the flow fields and the parameters of the particle impact. After the tests were carried out, it was concluded that the size of the particles, the diameter of the spray hole of the injector, and the pressure discrepancy between the gas supplying the powder and the main working gas led to a significant influence on the distribution of the particles both near the neck of the spray nozzle and in front of the substrate. Figure 7 illustrates how the particle deposition range on the substrate grows as the injector's inner diameter decreases. In addition, as the injector's inner diameter grows, so does the gradient of the particle departure from the nozzle axis upstream of the nozzle. As a result, the powder injector with a smaller inner diameter can, in the CSAM process, not only increase the production accuracy of parts but also, to a certain extent, lessen the likelihood of nozzle blockage or sticking upstream of the nozzle [22,23].

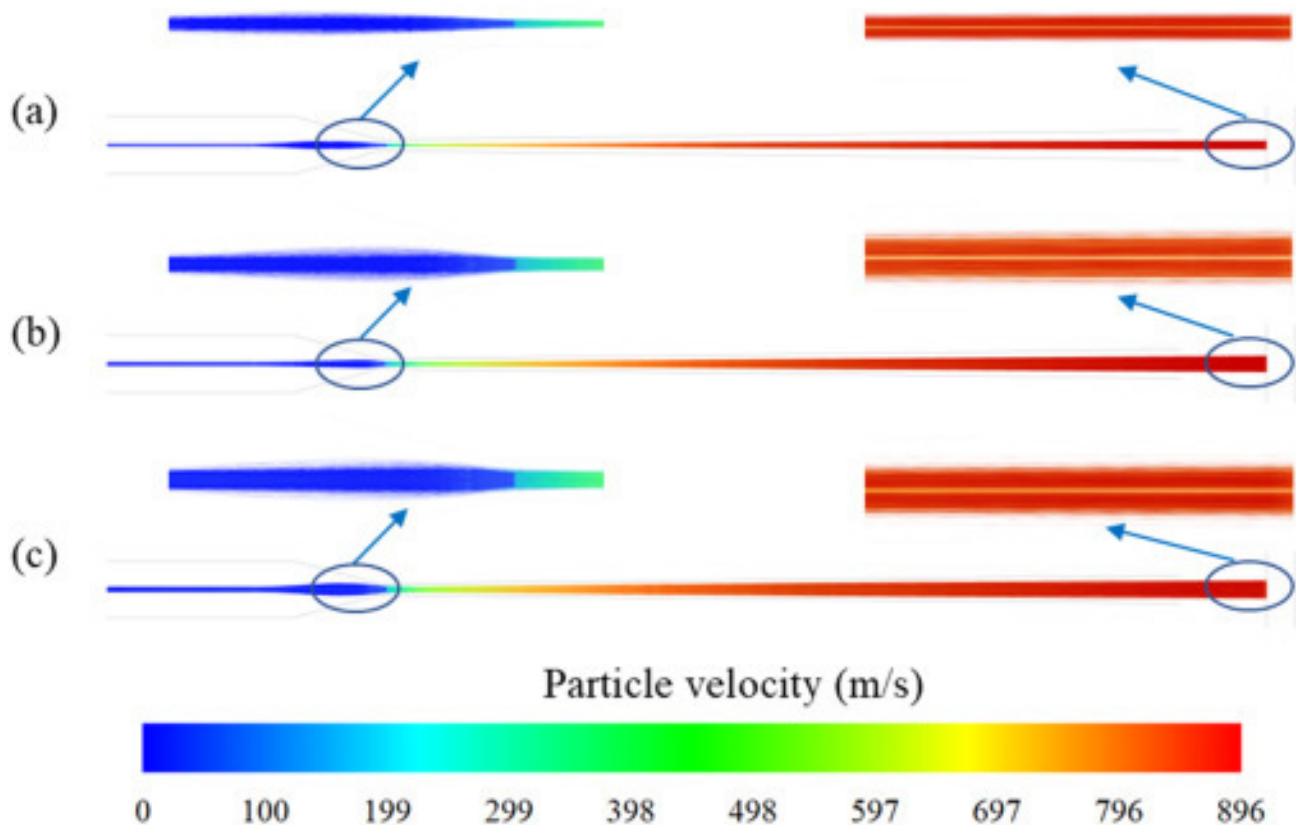


**Figure 7.** Particle tracks at different inner diameters of the powder injector are colored according to the particle velocity: (a) 0.5 mm; (b) 1 mm, and (c) 1.5 mm. The sizes of the particles range from 5 to 60  $\mu\text{m}$  [22].

Through these tests, it was highlighted that the improvement of the impact speed of the particles, as well as a reduction in the risk of clogging the nozzle with a concentration of particles near it, are optimized by reducing the internal diameter of the powder injector and by using a pressure that is smaller than the differentials; at the same time, the use of particles with diameters between 20–40  $\mu\text{m}$  lead to an improvement in precision [22].

An important aspect of this surface spraying technology is that it expands the range of applications in terms of thermal spraying, something that is applicable in industries such as automotive, aerospace, medical, and petrochemical, helping to both produce and restore various components, such as defects processing, casting, and even the possibility of remaking the mold [24].

### 3. Properties Obtained by the Cold Spray Method

#### 3.1. Microstructural Properties of Coatings by the Cold Spray Method

Cold spraying technology, through certain dynamics which contribute to the performance of the components that are subjected to surface spraying, contributes both to the improvement of this process and to the improvement and optimization of the powders in order to obtain microstructures with superior properties that to meet the needs of the industry.

In a study carried out by Jun et al., in which, through the cold spraying technique, coatings that were based on Ti-6Al-4V (Ti64) were made on a Ti-6Al-4V substrate, microstructural evolution (that starts from the powder as a raw material, up to the coating as a result of the deformation with a high deformation rate was observed. At the interface, the microstructure is noticeably different from the microstructures of the powder and the coating. Near the surface (both in the substrate and in the particles), narrow regions were observed represented by grains of a nanometric size; this remark was concluded from the

fact that adiabatic shear instability is observed with localized deformation showing a high deformation rate, along with a build-up of heat. The drastic change in the microstructure of the particle is due to the high-velocity impact during the cold spraying process that leads to a smaller grain size (<50 nm) on both sides of the particle periphery (<50 nm on the periphery and 200 nm in the middle of the particle), and on the above the particle, located away from the impact center, martensitic structures are found. As can be seen, Figure 8a represents an HRTEM image where the particle–substrate interface near the edges of the particle can be observed. The inset “p” and “s” shows the distribution corresponding to the particle area and also to the substrate area that are adjacent to the interface. Figure 8b represents the HRTEM image corresponding to the bonding region (area highlighted with square “T”) in Figure 8a, with an inset showing the diffractogram corresponding to this region [25–27].

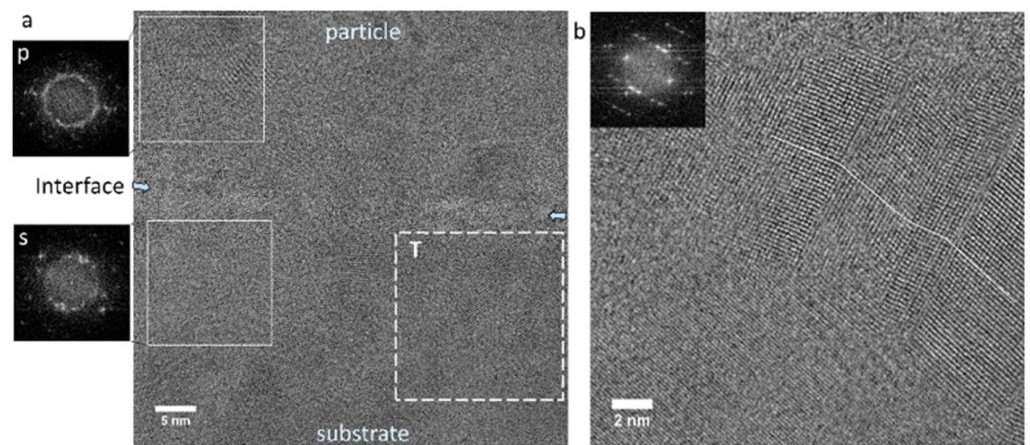


**Figure 8.** HRTEM images; (a) shows the particle-substrate interface and (b) shows the bonding area [27].

In Figure 9, following the cold spraying process, a schematic illustration of the microstructure of the particles from a coating near the substrate that shows the tiny grains as small circles, the coarser grains as big circles, and the martensitic structure by lines [27], is presented.

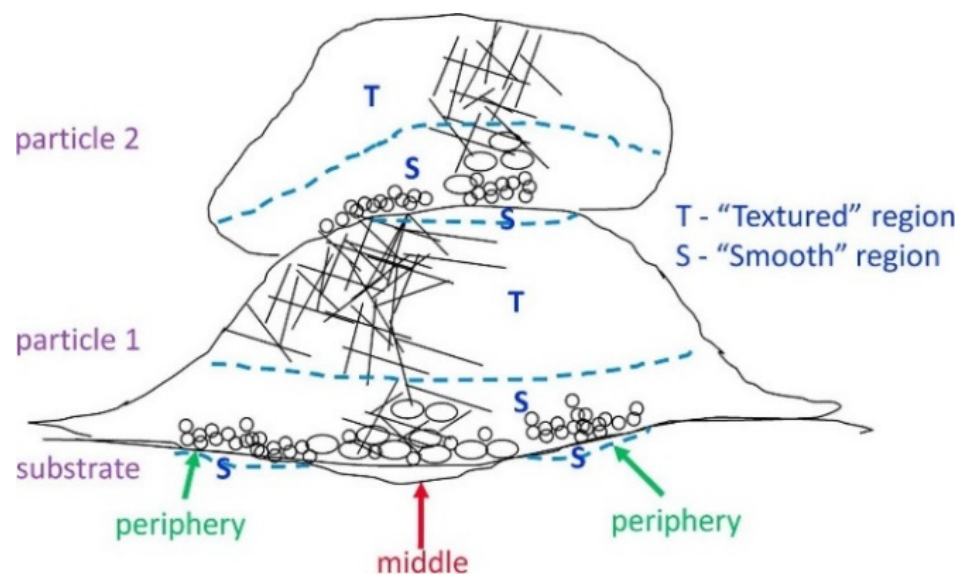


**Figure 9.** The microstructure of the particles seen with the aid of the schematic representation [27].

Through an overview, the morphology of the deposited particles is exposed, and it can be observed that most of the particles are strongly deformed and flattened. Textured and smooth regions can be observed in most of the particles, and the volume ratio between these regions is influenced by the speed and size of the particles but also by the point of impact on the previous deposits. Figure 10 shows an unengraved cross-section; Figure 10a represents the coating–substrate interface, and Figure 10b shows the inner region, with “T” indicating the textured region and “S” indicating the smooth region [27].

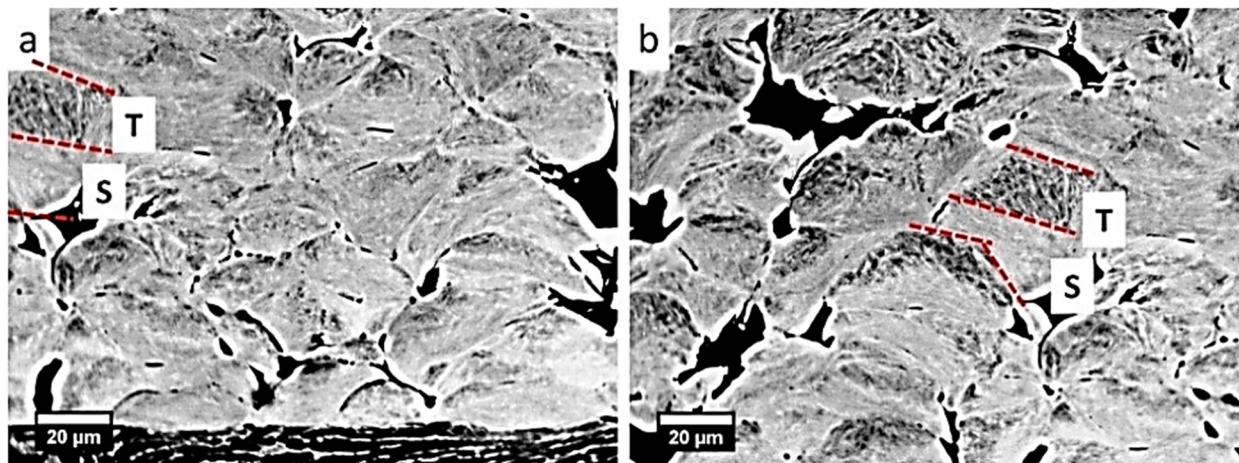


**Figure 10.** Cross section Ti-6Al-4V (Ti64) coating. (a) Coating–substrate interface; (b) inner region [27].

### 3.2. Mechanical Properties of the Coatings of the Cold Spray Method

Through the multitude of improvements it brings (through surface spraying), the cold spraying method manages to confer mechanical characteristics that not only manage to satisfy specific needs in terms of the restoration of various components but also confer new parts that are required on the surface (with a functional role or not), depending on the needs, to present a dense, very hard layer.

Goanta et al. [28,29] conducted a fatigue analysis of a base material–coating material assembly, including a morphological analysis of crack initiation at the interface of the two materials, using AISI 4340 and AISI 52100 alloy steel with a WIP-C1 commercially available powder (by cold-spray technique). The study presented results at fatigue stress levels below 340 MPa, with neither the tested substrate nor the coating incurring any damage after 5 million cycles. The stress values between 350 MPa and 370 MPa caused less coating damage, and the components could be used within this stress range without impacting the base material or coating assembly. In the region of sudden crack propagation, detachments of the coating material from the base material may be detected at pressures exceeding 370 MPa.

Lioma et al. performed a study on the hardness obtained by deposition in which cold spraying is used at low pressures using WC-Ni and WC-12Co-Ni powders with different percentages of Ni (4, 10, 25, and 50% Ni) on a mild steel. After the tests were performed and the results obtained by SEM and XRD were analyzed, it could be observed that, while the deposit was forming, by means of the good refinement of the grains and the rather small porosity (up to 1, 47%) (and at the same time, with a small percentage of Ni, for coatings with another percentage, namely WC—4% Ni and WC-12Co—4% Ni), leads to obtaining an increased hardness, and from the total of eight combinations performed for WC-Ni powder and WC—4% Ni, respectively, a hardness of 459.2 HV03 was obtained; however, this value is not quite satisfactory if it is compared with the average values generally obtained by other coating methods, such as CGDS and HVOF, reaching values of approximately 1135 HV03. The microstructures showing the compositions of WC-Ni (Figure 11a–d) and WC-12Co-Ni (Figure 11e–h) (the white phase represents WC, light gray

Co, and dark gray Ni matrix), are shown in Figure 11, and the properties of the coatings resulting from the tests performed are presented in Table 3 [30].

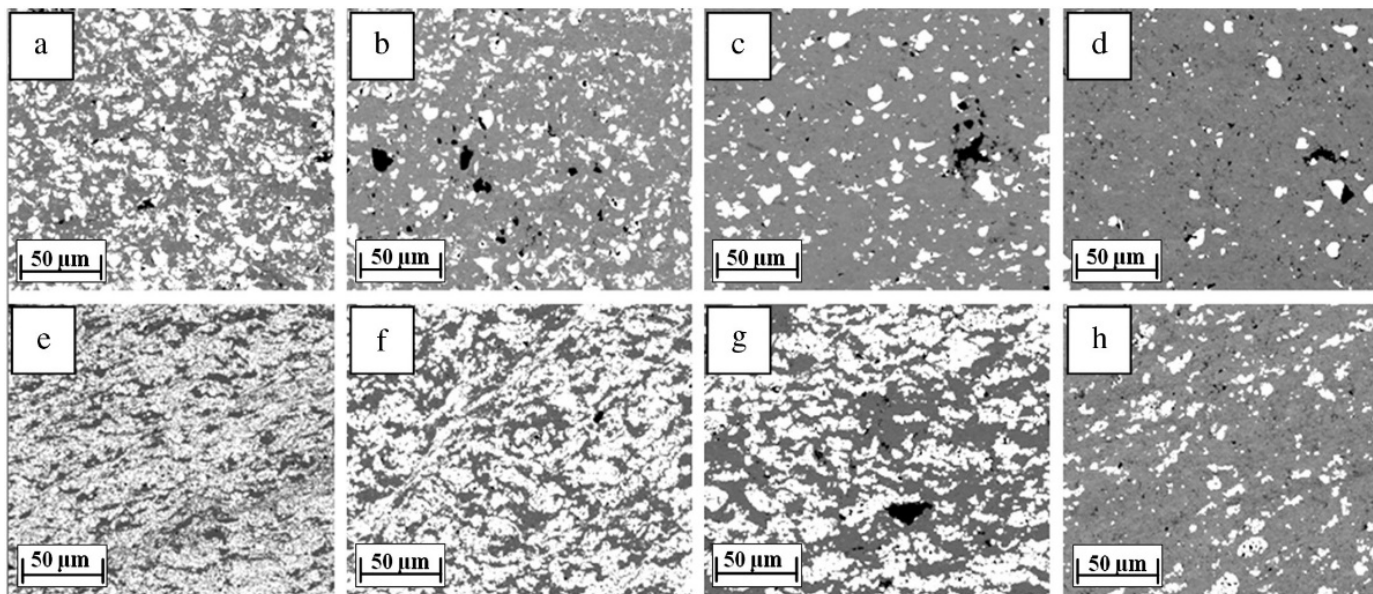
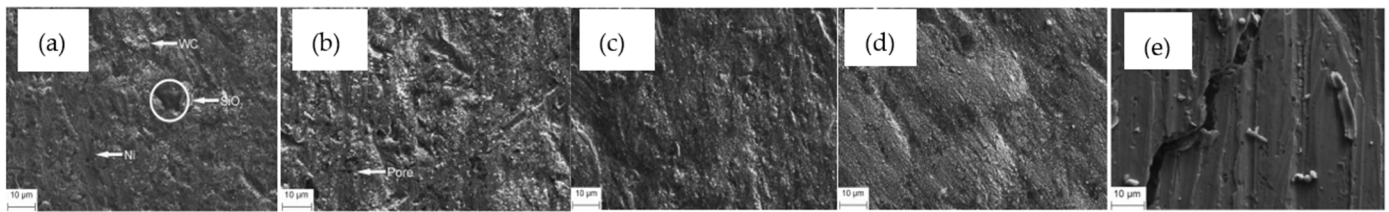


Figure 11. The microstructure by cold spray deposition: (a–d) microstructures with the composition WC-Ni; (e–h) microstructures with the composition WC-12Co-Ni [30].

Table 3. Properties of coatings [30].

Ni (%)	Hardness (HV <sub>0.3</sub> )		Porosity (%)		Binder Mean Free Path (µm)		WC Retained (%)	
	WC	WC12Co	WC	WC12Co	WC	WC12Co	WC	WC12Co
4	459 ± 19	414.9 ± 23.2	1.47	3.51	5.42	1.77	39.89	74.08
10	391.5 ± 16.1	362.2 ± 32.6	2.27	3.15	12.54	3.10	24.47	63.54
25	305.6 ± 17.0	294.3 ± 31.6	2.70	3.79	21.21	4.85	17.07	47.92
50	275.8 ± 16.3	260.9 ± 25.4	2.49	5.11	48.59	10.09	6.92	27.06

N.M. Melendez et al. carried out research regarding the wear behavior of a steel substrate with a low carbon content of tungsten (WC) and Ni deposits and a metal matrix made by means of cold spraying technology with low pressure; the WC percentage of these WC-Ni deposits being 7%, 19%, 56%, and 66%, respectively. At the same time, these deposits were made with pure nickel and were then subjected to a test wear standard: ASTM G65 dry abrasion. After the interpretation of the results, it was concluded that the WC samples showed a significant decrease in wear determined by the increase in the percentage of WC, from which it was concluded that the improvement in wear is obtained by increasing the amount of WC; on the sample deposited with pure nickel, as can be observed by the growths in the crack network, the lack of WC reinforcement was harmful. The worn surfaces of the samples deposited with 7% WC (Figure 12a), 19% WC (Figure 12b), 56% WC (Figure 12c), and 66% WC (Figure 12d), and also the worn surfaces with pure nickel deposits (Figure 12e) are presented in Figure 12; a cross-section of the worn coating is shown in Figure 13 [31].



**Figure 12.** Worn surface of WC-Ni coatings and pure nickel coatings: (a) 7% WC; (b) 19% WC; (c) 56% WC; (d) 66% WC; (e) pure nickel [31].

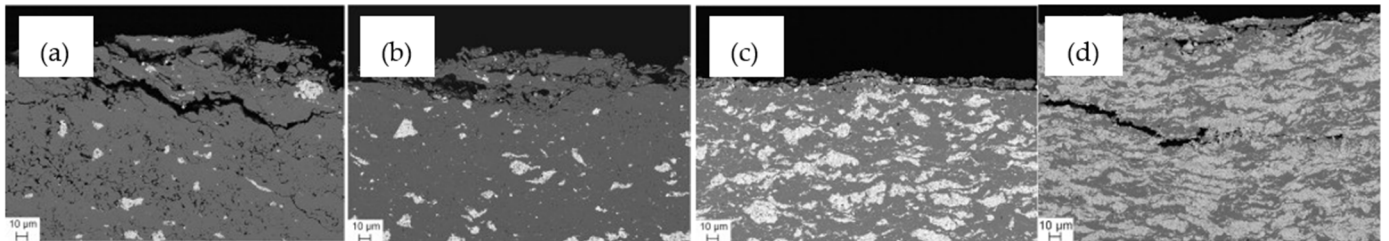


**Figure 13.** Cross-section of WC-Ni MMC coating worn with (a) 7% WC; (b) 19% WC; (c) 56% WC; (d) 66% WC [31].

### 3.3. Corrosion Resistance Properties of Coatings by the Cold Spray Method

The use of the cold spraying method and the multitude of types of powders that can be used depending on the different destinations for which they are created and optimized can create coatings that, in addition to the other properties they incorporate, manage to perfect the components against the so-called corrosion phenomenon, which, over a shorter or longer time, can produce effects that are sometimes capital for the various components, such that, through the superficial spraying, not only is it restored but it is also given a superficial protective layer that is resistant to corrosion.

Silva et al. carried out a study regarding the improvement of the properties of corrosion behavior via cold-sprayed WC-Co deposits on an aluminum alloy: AA 7075-T6, where, by means of the alloying elements such as Mg, Zn, and Cu, the susceptibility to corrosion is high. The research was carried out on different samples deposited with WC-12Co and WC-25Co. Regarding the WC-12Co sample, the results led to obtaining a corrosion resistance for a time of 400 h of immersion in a 3.5% NaCl solution and for even longer immersion times, through the dissolution of the cobalt phase and at the same time through the loss of WC particles, it led to the formation of interconnected porosities, such that the access of the electrolyte could be allowed, and therefore the corrosion of the substrate and the other sample (deposition with WC-25Co), led to very good results in terms of AA protection. Regarding alloy 7075-T6 against corrosion, the sample managed to exceed 700 h of immersion in 3.5% NaCl solution; when testing the sample with exposure to salt spray with neutral NaCl 5%, the sample showed resistance to exposure for 3000 h. The cross-sectional image after these tests is shown in Figure 14 [32].

Small amplitude linear polarization measurements made after 18 h in a 3.5% NaCl solution were utilized to estimate the values of RP for the substrate and coated samples, and the corrosion-current densities were calculated using these values. Additionally, the  $E_{\text{corr}}$  and  $i_{\text{corr}}$  values calculated using the Tafel plot extrapolation method from the potentiodynamic polarization curves are presented in Table 4 (a:  $i_{\text{corr}}$  values were calculated using the Stern–Geary equation, where  $i_{\text{corr}} = ba/2.3 R_p$  and  $ba$  is the polarization resistance and  $b$ : values for  $i_{\text{corr}}$  that were acquired by extrapolating from Tafel plots).

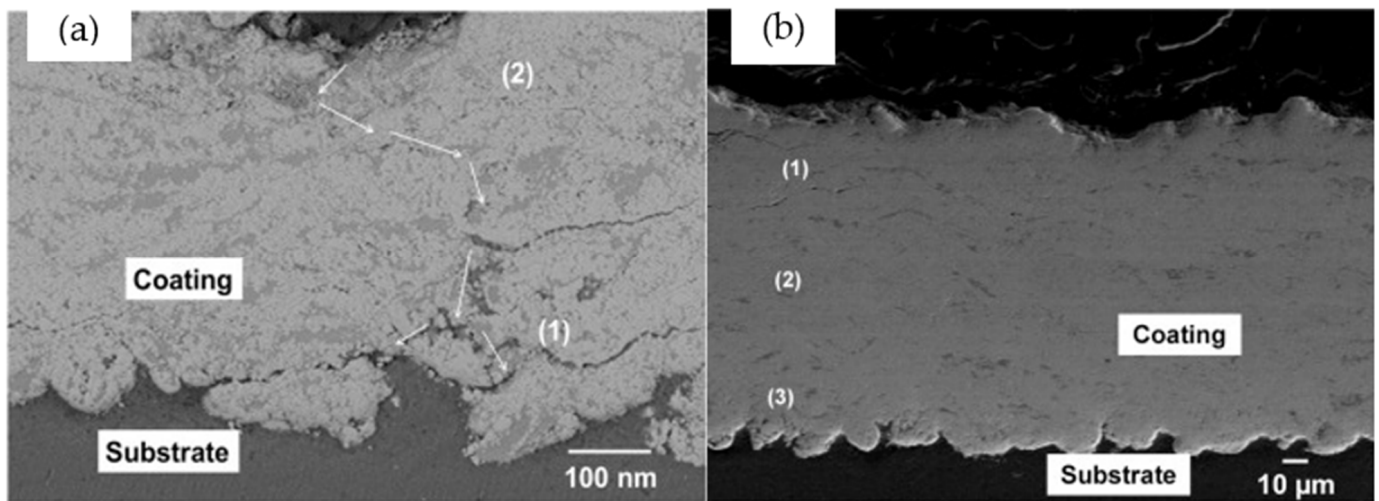


**Figure 14.** Cross-sectional image (SEM) of (a) WC-12Co coating after 600 h and (b) WC-25Co coating after 700 h of 3.5% NaCl immersion [32].

**Table 4.** Corrosion characteristics calculated using potentiodynamic polarization and small amplitude linear polarization curves following an 18 h immersion in a 3.5 wt% NaCl solution [32].

Parameter	AA 7075-T6	WC-12Co	WC-25Co
$E_{i \rightarrow 0}$ (mV vs. Ag   AgCl   KCl <sub>3 mol/L</sub> )	$-814 \pm 2$	$-326 \pm 4$	$-425 \pm 2$
$E_{corr}$ (mV vs. Ag   AgCl   KCl <sub>3 mol/L</sub> )	$-831 \pm 2$	$-336 \pm 2$	$-425 \pm 1$
$^a i_{corr}$ ( $\mu\text{A cm}^{-2}$ )	10.7	28	30
$^b i_{corr}$ ( $\mu\text{A cm}^{-2}$ )	2.9	10	23
$b_a$ (mV dec <sup>-1</sup> )	82.5	148	111

The substrate and coating anodic polarization curves are shown in Figure 15. The  $E_{corr}$  and  $i_{corr}$  values for AA 7075-T6 were 0.8 V vs. Ag | AgCl | KCl<sub>3 mol/L</sub> and 2.5 A cm<sup>2</sup>, respectively. The polarization curve for the substrate is shown in Figure 15a. Pitting corrosion caused the current to spike when the potential reached 0.70 V vs. Ag | AgCl | KCl<sub>3 mol/L</sub>. The cathodic curves produced in the presence of oxygen are shown in Figure 15b. These curves revealed two current plateaus that were ascribed to a reduction in oxygen in the range of  $-0.5$  to  $-0.9$  V vs. Ag | AgCl | KCl<sub>3 mol/L</sub> and to a reduction in water at greater negative potentials. The cathodic curves produced in the absence and presence of oxygen are compared in Figure 15c. While the predominant process in the absence of oxygen was the reduction in water and the evolution of hydrogen, the introduction of oxygen caused a quick electrochemical reaction that was diffusion-controlled [32,33].

Following a review by Ashokkumar et al. on sputtering technology and its corrosion benefits, their review concludes that the benefits of low particle temperatures in this sputtering process result in a decrease in the degree of corrosion on the coated surface, which is a big improvement when compared to the other technologies (HVOF and APS). From the approach of this paper on the technological process of cold thermal spraying, the idea emerges that this process has the potential to dominate the sector of thermal spraying technologies in industries such as the aerospace, marine, and automotive industries in the coming years [34,35].

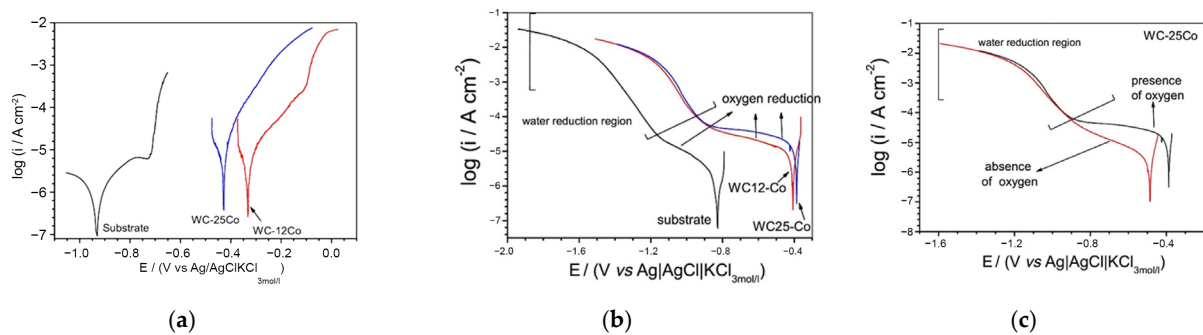


**Figure 15.** (a) Anodic and (b) cathodic potentiodynamic polarization curves for AA 7075-T6 alloy and the coated samples, recorded at  $0.166 \text{ mV s}^{-1}$  in quiescent 3.5 wt% NaCl solution after approximately 18 h of immersion. (c) The WC-25Co coating cathodic curves obtained in the same solution with and without oxygen [32].

In research conducted by Zhang et al. for the purpose of repairing flaws and preventing the corrosion of AA2024-T3, thick Al-based coatings were effectively coated, utilizing the low-pressure cold spray approach. In order to create improved shot peening effects, spherical  $\text{Al}_2\text{O}_3$  particles were added to the feedstock materials. Based on the results of the cyclic polarization studies, it can be concluded that the tested coatings' primary corrosion form was pitting. Following the analysis regarding the comparison of the three depositions, the Al 2024 coating presented the weakest result, while the CP Al coating led to the strongest pitting resistance and passivation capacity. According to the SVET data, after 24 h of immersion in a 3.5% NaCl aqueous solution, the CP Al coating showed the lowest pitting activity, while the Al 2024 deposition showed the most. The Al 2024 coating showed the highest corrosion rate throughout the EIS tests in a 3.5% NaCl aqueous solution. The Al 5083 coating resulted in the lowest corrosion rate once the CP Al coating test was completed. As seen in Figure 16, the corrosion behavior of the cold-sprayed coatings was investigated. According to Figure 16a, the pitting location on the CP Al coating's surface is substantial, deep, and has an uneven form. One spherical  $\text{Al}_2\text{O}_3$  particle is found at the pit's edge, and no preferential Al matrix dissolving is shown at the Al- $\text{Al}_2\text{O}_3$  interface, which shows that no galvanic cell was formed between the Al matrix and the  $\text{Al}_2\text{O}_3$  particle. In addition, a layer of corrosion products has developed on the matrix, which can partially isolate the electrolyte coating. On the surface of the Al 2024 coating, there are multiple pits of relatively small depths that are randomly positioned, as seen in Figure 16b. When comparing the pits on the Al 5083 coating to those on the CP Al coating, Figure 16c demonstrates that the Al 5083 coating pits are shallow and smaller in size [36].

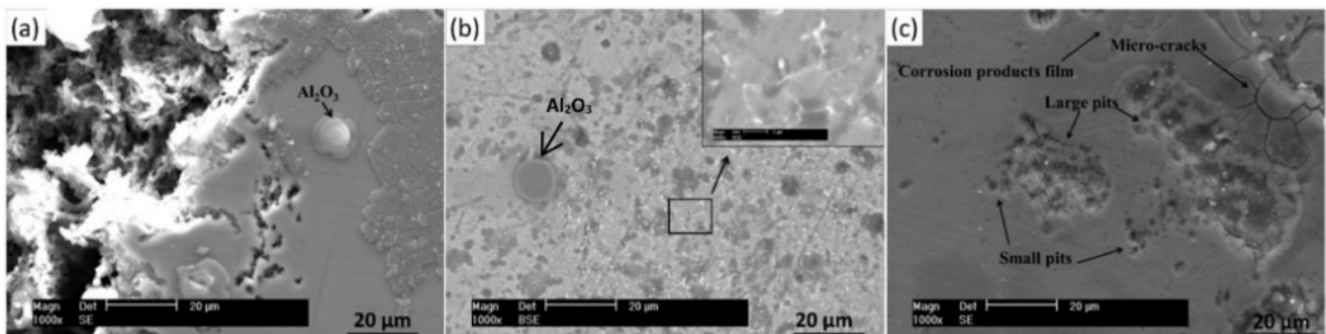


**Figure 16.** Surface morphology of the CS coatings following CP corrosion test: (a) represents the Al coating, (b) represents the Al 2024 coating, and (c) represents the Al 5083 coating [36].

Figure 17 displays the cyclic polarization curves. Possible scan routes are shown by the solid arrows adjacent to the forward and reverse anodic branches. At a certain critical potential, known as the pitting potential  $E_{\text{pit}}$ , where a sharp increase in anodic

current occurs as a result of the breakdown of the passive film and the beginning of pitting corrosion, the corrosion currents of the Al and Al 5083 coatings decreased rapidly with the increase in potential and reached the minimum at their  $E_{\text{corr}}$ , respectively. However, when the potential increased to the  $E_{\text{corr}}$ , the corrosion current of the Al 2024 covering fell at a very slow pace. The current then immediately increased sharply after that.  $E_{\text{pit}}$  may be a useful option to show corrosion-resistance since more pitting potential often equates to better resistance to pitting corrosion [36–38].

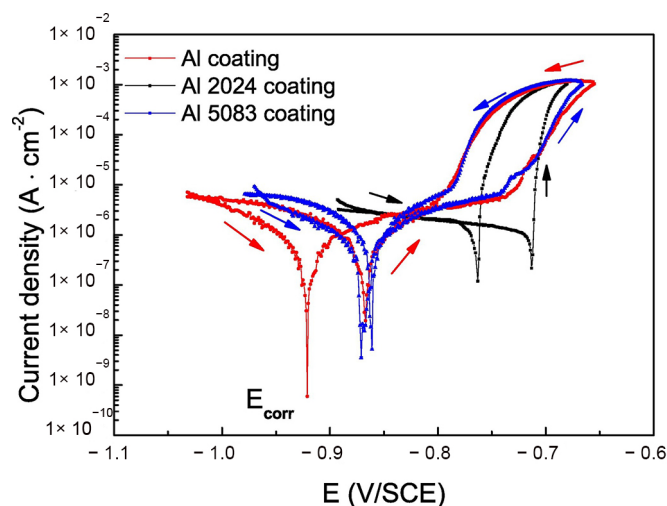


**Figure 17.** After 6 h of immersion in a 3.5 wt% NaCl solution, coated samples' cyclic polarization was measured at 1 mV/s [36].

### 3.4. Potential Applications Using the Cold Spray Method

Cold spraying technology, through the fact that it succeeds in improving the properties of the materials leading to an improvement in the characteristics and functionality of the various components that are subject to this process, and more than that, through the possibility of the deposition on a wide range of materials, such as metals, ceramics, polymers, etc., manages to gain value and be used in numerous industries, such as the energy sector, in order to extend the life of boilers damaged by corrosion and oxidation from the high temperatures of thermal power plants; cold spraying in the aerospace industry manages to restore and repair numerous defective parts that are rejected in the technological manufacturing process because they present very high-quality standards, returning the parts to the desired characteristics; in the biomedical sector, cold spraying manages to lend itself to the possibility of depositing on different types of orthopedic and dental implants through coatings (for example, with hydroxyapatite and titanium (ceramic coatings)) that improve osseointegration, etc., [39–41].

In a study by Yongming et al. on HEA composite coatings where FeCoNiCrMn HEA composite coatings reinforced with  $\text{Al}_2\text{O}_3$  (11 and 20 wt%  $\text{Al}_2\text{O}_3$ ) particles were created by cold spraying showed that cold spraying represents a potential approach for creating HEA composite coatings. The interface between the substrate and the coatings as they were applied can be seen in Figure 18a–c (SEM images). It can be seen that all of the coatings demonstrated strong bonding with the aluminum alloy substrates, as evidenced by the smooth interface devoid of gaps and fractures. Along the contact between the substrate and coating, a mechanical, interlocking phenomena was visible. The substrate material firmly trapped certain particles that managed to pierce it. When hard FeCoNiCrMn particles strike soft substrate material, there is a strong plastic deformation that leads to the development of mechanical interlocking. A prominent feature of cold-sprayed coatings is mechanical interlocking, which can provide the coatings with strong adherence. The cross-sectional SEM images of the as-deposited coatings are shown in Figure 18d–f. The FeCoNiCrMn coatings are clearly shown to have a dense microstructure with fewer pores, as indicated by the yellow arrows, and interparticle boundaries, indicated by the red arrows. As seen in

Figure 18e,f, the composite coatings also feature a thick microstructure. The white arrows indicate where in the FeCoNiCrMn matrix the  $\text{Al}_2\text{O}_3$  particles were evenly distributed. The red arrows indicate the interparticle gaps, increasingly noticeable for a higher percentage of  $\text{Al}_2\text{O}_3$  [42].

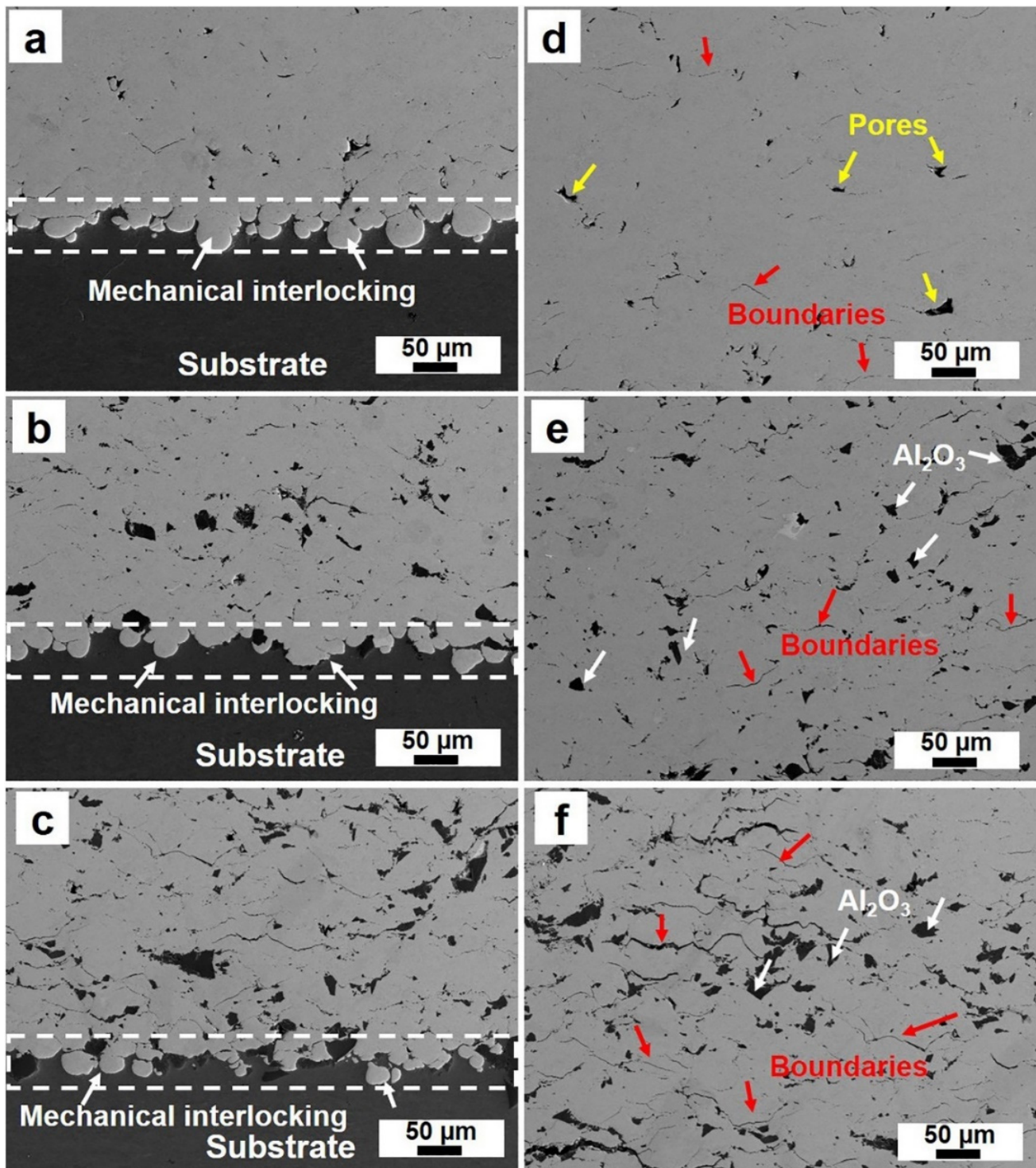


**Figure 18.** SEM pictures of the coating–substrate interfaces and coatings in the cross-section. Pure FeCoNiCrMn coating is shown in (a,d), whereas (b,e) shows an 11 wt%  $\text{Al}_2\text{O}_3$  coating, and (c,f) a 20 wt%  $\text{Al}_2\text{O}_3$  coating [42].

Within the US Army, Aaron et al. have carried out several pieces of research regarding the potential of using the cold spraying technique in order to restore (and, at the same time, improve) the characteristics of some components in the military environment using WIP powders. In the conducted research, different types of powders were used, namely WIP-BC1 powders as the base substrate, and after this substrate, the final layer was made with WIP-C1 powder; the tested component was made from AISI alloy steel 4340. Following the interpretation of the results, it was concluded that the wear performance increased significantly, being superior even to chrome plating, with a good resistance to impact demand, and the performance of the shear tests managed to obtain very good results in terms of an increase in hardness, namely, an increase in hardness from 17 HRC (as shown by the base material) to 40–44 HRC. Regarding the porosity of the surface, the results are very satisfactory, obtaining values of 1.5–3% in the case of spraying with nitrogen and below 1% in the case of using helium. The surface sprayed with the WIP-C1 powders, as well as the bonding substrate in which the WIP-BC1 powders were used, are shown in Figure 19, and the part used in the spraying process is shown in Figure 20 [43].

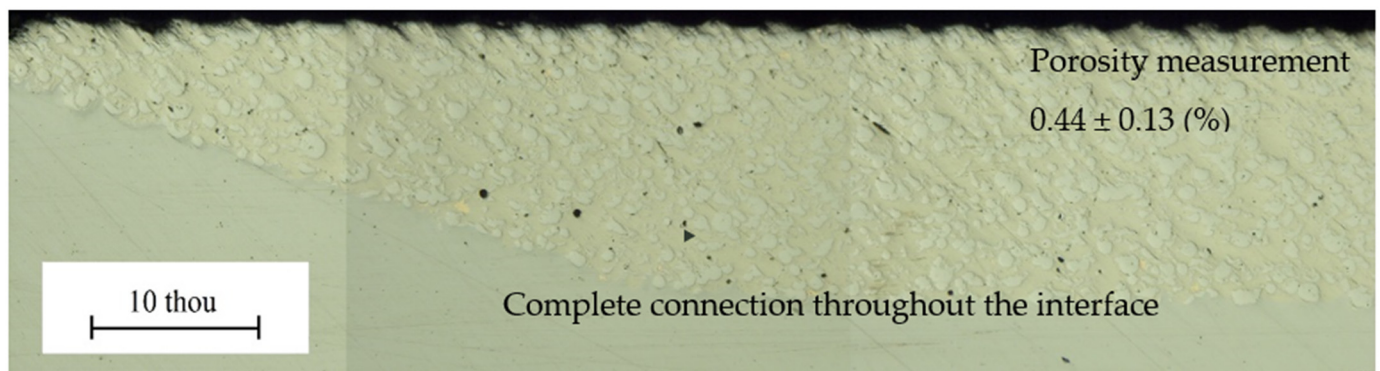


Figure 19. Sprayed surface using WIP-BC1 powders and WIP-C1 powders [43].

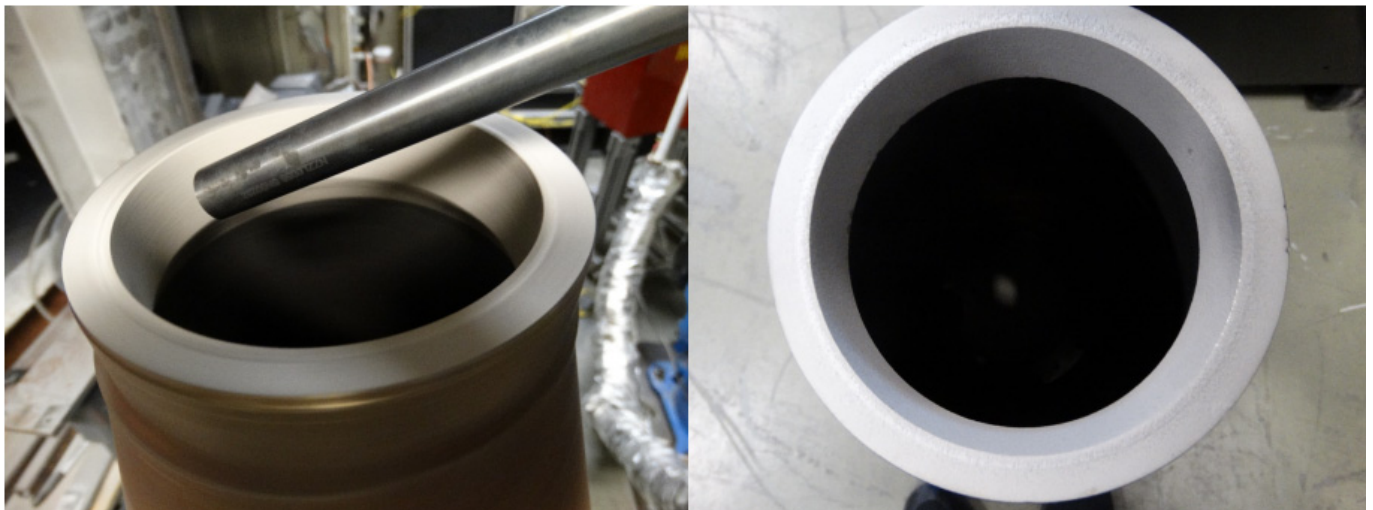
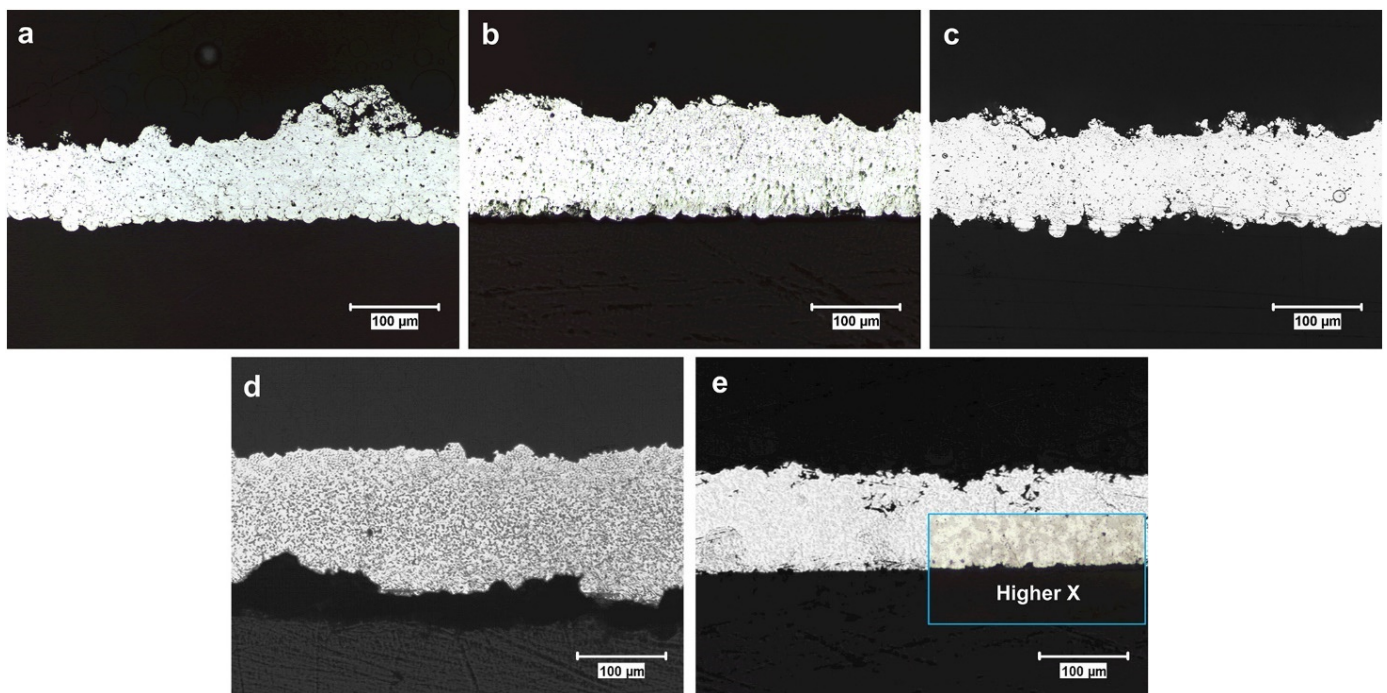


Figure 20. Turret mount (Bradley) cold sprayed [43].

The effectiveness of this technology in terms of technological procedures for mending different components leads to the ongoing improvement of both the spraying technology and the powder utilized in this process.

In a piece of research conducted by Hanqing et al., the powders of SnZn and SnBi with lower melting points than Sn were cold sprayed onto polymeric substrates (ABS, Nylon, PC, and PE și PP). Due to a larger degree of particle melting, the results demonstrate that lowering the melting temperatures of the feedstock powders can increase their deposition

efficiency on polymeric substrates. The high-toughness, extremely high molecular weight polyethylene and polycarbonate were two of the five polymers that were most challenging to metalize. The metal coatings on the polymer substrates are shown in cross-sections in Figure 21. The SnZn coatings cold sprayed at 300 °C and 80 psi are shown for ABS, Nylon, and PP; for UHMW and PC, the SnBi coating at 300 °C and 42 psi is displayed because the deposition of SnZn was insufficient or irregular on these latter two polymers. The two-phase microstructure that is present in the feedstock powder is still present in all of the coatings, which are all rather consistent in thickness and density. Because the spherical particle can be observed penetrating into the substrate for the SnZn coatings on ABS, Nylon, and PP, mechanical interlocking can be seen. The combined impact of glass transition temperature and strength may be used to explain why the degree of interface waviness is in the order of PP-ABS-Nylon. The ease of penetration and interlocking increases with decreasing strength. Since mechanical interlocking and particle penetration are challenging, the low DE of Sn and SnZn for the two polymers with high toughness, UHMW and PC, is comprehensible. The top substrate surfaces are comparatively smooth when UHMW and PC are metalized with SnBi, indicating that there is less mechanical interlocking (details of the SnBi-PC interface are shown by the high magnification inset). The coating on UHMW does, in fact, exhibit delamination. The extensive melting of the particles and the low gas pressure at 300 °C prevent mechanical anchoring for SnBi [44–47].



**Figure 21.** Cross-sections of cold-sprayed SnZn ((a–c) 80 psi) and SnBi ((d,e) 42 psi) coatings on all polymers at 300 °C are shown in the optical micrographs below: (a) ABS, (b) Nylon, (c) PP, (d) UHMW, and (e) PC [44].

#### 4. Discussion

Since the efficiency of the deposition process is strongly influenced by a combination of the mechanical properties of the powder and the substrate materials, producing thick coatings can be challenging in certain circumstances due to the fact that the mechanical properties of the raw material powder and materials of the substrate work together; at the same time, low-porosity coatings are made possible by the cold spray method, while maintaining the phase composition of the raw material powder, although, in this process, the particles are subjected to high-speed deformation when in contact with the substrate or previous deposit, resulting in significant changes in the microstructure of the particle. It

is worth mentioning that the temperature of the working gas during CS is always lower than the melting point of the sprayed material, with cold-sprayed coatings reducing or even completely eliminating oxide formation and thermal stresses compared to thermally sprayed coatings.

Regarding improvements to the properties of various materials that present high properties, such as steels for the construction of armor, steels for the construction of bearings, and other types of components that are subject to extreme operating conditions, in terms of improving wear resistance, for example, an increase in layer resistance is obtained by applying FSP on a WC-12%Co coating that is thermally sprayed onto 52100 steel. In order to create a dense structure with a higher hardness after FSP, this included the decomposition of the particles of sprayed WC and, subsequently, the easier dispersion of smaller WC particles. At the same time, the performance that can be observed even in some military components that were subjected to cold spraying using WIP-C1 powders, are constituted by an increase in hardness from a value of 17 HRC (as the base material), up to 40–44 HRC after spraying. In the dry abrasion tests (ASTM G65) performed on other types of materials that were subjected to cold spraying, it was observed that the wear rate decreased considerably at higher concentrations of WC, which resulted in the fact that the coating with a higher WC concentration had the least wear.

Due to the fact that, in terms of lifetime properties, corrosion behavior plays a decisive role, from the documentation accumulated within this manuscript, the tests have shown that the CGS technique has very high potential as it can protect AA 7075T6 from corrosion for at least 700 h of immersion in 3.5% NaCl solution and for 3000 h in a salt spray test with 5% (by weight) neutral NaCl at 35%, indicating very high performance against corrosion under these circumstances. The WC-12Co coating showed corrosion resistance after spending at least 400 h immersed in a 3.5% NaCl solution.

## 5. Conclusions

Through the uniqueness of the characteristics it incorporates, cold spraying technology leads to an improvement in material properties, and, following numerous studies carried out on this technique, it was concluded that by processing the particles in a solid state, they adhere to the surface instead of eroding.

52100 steel is characterized by the high potential it possesses through the chromium alloy and its high carbon content, thus being able to present ideal properties in terms of its use for various components that are subjected to very high demands. Its properties are enhanced by surface deposits, resulting in a longer life both through increased corrosion resistance and a high level of hardness.

Cold spraying proves to be an effective technique to improve material properties, and this is confirmed by its integration into different fields of industry, where it is competitive due to the fact that it is the only technique in which the particles are deposited below the melting point.

For compact coatings, it would be useful to emphasize the optimization of the process parameters, including nozzle design. Ensuring the improvement of the process parameters is useful for the application of thick, uniform, and consistent layers.

Among the many spraying technologies, CS cladding is a highly efficient and cost-effective method for adding composite layers with superior properties to a wide range of materials, including metals, composites, and polymers.

However, it cannot be neglected that, although cold spraying is a promising approach, it presents challenges in terms of the costs of this process; the main cost factors are the raw material powder and the high gas consumption rate. Helium provides a high-quality microstructure and excellent deposition efficiency but is expensive. On the other hand, the use of nitrogen is a fairly cost-effective alternative.

**Author Contributions:** Conceptualization, F.C.L., C.M. and A.C.S.; methodology, B.I.; software, A.C.S.; validation, C.M., A.C.S. and B.I.; formal analysis, V.N.A.; investigation, F.C.L.; resources, C.M.; data curation, B.I.; writing—original draft preparation, F.C.L. and B.I.; writing—review and editing, C.M., A.C.S. and V.N.A.; supervision, C.M. All authors have read and agreed to the published version of the manuscript.

**Funding:** This research received no external funding.

**Data Availability Statement:** Not applicable.

**Conflicts of Interest:** The authors declare no conflict of interest.

## References

1. Cristea, S. Contributii la Studiul Comportarii Unor Materiale de Blindaj la Impactul cu Proiectilul. Ph.D. Thesis, Lucian Blaga University, Sibiu, Romania, 2008.
2. Phillips Federal News. Available online: <https://phillipscorp.com/federal/2020/06/24/vrc-army-phillips-federal/> (accessed on 6 September 2022).
3. Shikalov, V.S.; Vidyuk, T.M.; Filippov, A.A.; Kuchumova, I.D. Microstructure, mechanical and tribological properties of cold sprayed Cu-W coatings. *Int. J. Refract. Met. Hard Mater.* **2022**, *106*, 105866. [\[CrossRef\]](#)
4. Wei, F.J.; Chou, B.Y.; Fung, K.Z.; Tsai, S.Y. Thermomechanical properties of cold-sprayed copper coatings from differently fabricated powders. *Surf. Coat. Technol.* **2022**, *434*, 128128. [\[CrossRef\]](#)
5. Ranjan, R.; Das, A.K. A review on surface protective coating using cold spray cladding technique. *Mater. Today Proc.* **2022**, *56*, 768–773. [\[CrossRef\]](#)
6. Poza, P.; Maneiro, M.A.G. Cold-sprayed coatings: Microstructure, mechanical properties and wear behaviour. *Prog. Mater. Sci.* **2022**, *123*, 100839. [\[CrossRef\]](#)
7. Champagne, V.K. *The Cold Spray Materials Deposition Process: Fundamentals and Applications*; Woodhead: Cambridge, UK, 2007; p. 376.
8. Neu, R.; Maier, H.; Boswirth, B.; Elgeti, S.; Greuner, H.; Hunger, K.; Kondas, J.; Muller, A. Investigations on cold spray tungsten/tantalum coatings for plasma facing applications. *Nucl. Mater. Energy* **2022**, *34*, 101343. [\[CrossRef\]](#)
9. Jan, C.; Monika, V.; Frantisek, L.; Martin, K.; Jan, K.; Reeti, R.S. Cold Sprayed Tungsten Armor for Tokamak First Wall. *Coatings* **2019**, *9*, 836.
10. Yeom, H.; Sridharan, K. Cold spray technology in nuclear energy applications: A review of recent advances. *Ann. Nucl. Energy* **2021**, *150*, 107835. [\[CrossRef\]](#)
11. SSAB. Available online: <https://www.ssab.com/en> (accessed on 7 September 2022).
12. Dwight, D.S.; William, A.G.; Matthew, S.B.; Stockman, R.K. *Balistic Testing of SSAB Ultra-High-Hardness Steel for Armour Applications*; Army Research Laboratory: Adelphi, MD, USA, 2008.
13. Olympicsteel. Available online: <https://www.olysteel.com/products/alloy/mil-dtl-46100-mil-a-46100-armor-steel> (accessed on 7 September 2022).
14. Poplawski, A.; Kedzierski, P.; Mork, A. Identification of Armox 500T steel failure properties in the modeling of perforation problems. *Mater. Des.* **2020**, *190*, 108536. [\[CrossRef\]](#)
15. Alloy Steel 52100. Available online: <https://continentalsteel.com/carbon-steel/grades/alloy-52100/> (accessed on 21 September 2022).
16. Panda, A.; Sahoo, A.K.; Kumar, R.; Das, R.K. A review on machinability aspects for AISI 52100 bearing steel. *Mater. Today Proc.* **2020**, *23*, 617–621. [\[CrossRef\]](#)
17. Kiranbabu, S.; Tung, P.Y.; Sreekala, L.; Prithiv, T.S.; Hickel, T.; Pippan, R.; Morsdorf, L.; Herbig, M. Cementite decomposition in 100Cr6 bearing steel during high-pressure torsion: Influence of precipitate composition, size, morphology and matrix hardness. *Mater. Sci. Eng. A* **2022**, *833*, 142372. [\[CrossRef\]](#)
18. Qin, Y.; Mayweg, D.; Tung, P.Y.; Pippan, R.H. Mechanism of cementite decomposition in 100Cr6 bearing steels during high pressure torsion. *Acta Mater.* **2020**, *201*, 79–93. [\[CrossRef\]](#)
19. Rahbar-Kelishami, A.; Abdollah-Zadeh, A.; Hadavi, M.M.; Benerji, A.; Alpas, A.; Gerlich, A.P. Effects of friction stir processing on wear properties of WC-12%Co sprayed on 52100 steel. *Mater. Des.* **2015**, *86*, 98–104. [\[CrossRef\]](#)
20. Agiwal, H.; Yeom, H.; Pocquette, N.; Sridharan, K.; Pfefferkorn, F.E. Friction surfacing and cold spray deposition for surface crack repair in austenitic stainless steels. *Mater. Today Commun.* **2022**, *33*, 104692. [\[CrossRef\]](#)
21. Yeom, H.; Dabney, T.; Pocquette, N.; Ross, K.; Pfefferkorn, F.E.; Sridharan, K. Cold spray deposition of 304L stainless steel to mitigate chloride-induced stress corrosion cracking in canisters for used nuclear fuel storage. *J. Nucl. Mater.* **2020**, *538*, 152254. [\[CrossRef\]](#)
22. Wan, W.; Li, W.; Wu, D.; Qi, Z.; Zhang, Z. New insights into the effects of powder injector inner diameter and overhang length on particle accelerating behavior in cold spray additive manufacturing by numerical simulation. *Surf. Coat. Technol.* **2022**, *444*, 128670. [\[CrossRef\]](#)
23. Lupoi, R.; Neill, W. Powder stream characteristics in cold spray nozzles. *Surf. Coat. Technol.* **2011**, *206*, 1069–1076. [\[CrossRef\]](#)

24. Singh, H.; Sidhu, T.S.; Kalsi, S.B.S. Cold spray technology: Future of coating deposition processes. *Frat. Integrità Strutt.* **2012**, *22*, 69–84. [[CrossRef](#)]
25. Wong, W.; Rezaeian, A.; Irissou, E.; Legoux, J.G.; Yue, S. Cold spray characteristics of commercially pure Ti and Ti-6Al-4V. *Adv. Mater. Res.* **2010**, *89–91*, 639–644.
26. Herrera, J.E.J.; Bousser, E.; Schmitt, T.; Klemberg, S.J.E.; Martinu, L. Effect of plasma interface treatment on the microstructure, residual stress profile, and mechanical properties of PVD TiN coatings on Ti-6Al-4V substrates. *Surf. Coat. Technol.* **2021**, *413*, 127058. [[CrossRef](#)]
27. Jun, Y.L.; Ayan, B.; Adrian, W.Y.T.; Wen, S.; Xu, S.; Wei, Z.; Pio, J.B.; Feng, L.; Rjia, L.; Teng, M.L.; et al. Understanding the microstructural evolution of cold sprayed Ti-6Al-4V coatings on Ti-6Al-4V substrates. *Appl. Surf. Sci.* **2018**, *459*, 492–504.
28. Goanta, V.; Munteanu, C.; Muftu, S.; Istrate, B.; Schwartz, P.; Boese, S.; Ferguson, G.; Moraras, C.I.; Stefan, A. Evaluation of the Fatigue Behavior and Failure Mechanisms of 4340 Steel Coated with WIP-C1 (Ni/CrC) by Cold Spray. *Materials* **2022**, *15*, 8116. [[CrossRef](#)] [[PubMed](#)]
29. Goanta, V.; Munteanu, C.; Muftu, S.; Istrate, B.; Schwartz, P.; Boese, S.; Ferguson, G.; Moraras, C.I. Evaluation of the Fatigue Behavior and Failure Mechanisms of 52100 Steel Coated with WIP-C1 (Ni/CrC) by Cold Spray. *Materials* **2022**, *15*, 3609. [[CrossRef](#)] [[PubMed](#)]
30. Lioma, D.; Sacks, N.; Botef, I. Cold gas dynamic spraying of WC-Ni cemented carbide coating. *Int. J. Refract. Met. Hard Mater.* **2015**, *49*, 365–373. [[CrossRef](#)]
31. Melendez, N.M.; Narulkar, V.V.; Fisher, G.A.; McDonald, A.G. Effect of reinforcing particles on the wear rate of low-pressure cold-sprayed WC-based MMC coatings. *Wear* **2013**, *306*, 185–195. [[CrossRef](#)]
32. Silva, F.C.; Cinca, N.; Dosta, S.; Cano, I.G.; Couto, M.; Guilemany, J.M.; Benedetti, A.V. Corrosion behaviour of WC-Co coatings deposited by cold gas spray onto AA 7075-T6. *Corros. Sci.* **2018**, *136*, 231–243. [[CrossRef](#)]
33. Couto, M.; Dosta, S.; Torrell, M.; Fernandez, J.; Guilemany, J.M. Cold spray deposition of WC-17 and 12Co cermets onto aluminium. *Surf. Coat. Technol.* **2013**, *235*, 54–61. [[CrossRef](#)]
34. Ashokkumar, M.; Thirumalaikumarasamy, D.; Thirumal, P.B. Influences of Mechanical, Corrosion, erosion and tribological performance of cold sprayed Coatings A review. *Mater. Today Proc.* **2021**, *46*, 7581–7587. [[CrossRef](#)]
35. Zhu, L.; Xu, B.; Zhou, M.; Hu, S.; Zhang, G. Fabrication and characterization of Al-Zn-Cu composite coatings with different Cu contents by cold spraying. *Surf. Eng.* **2020**, *36*, 1090–1096. [[CrossRef](#)]
36. Zhang, Z.; Liu, F.; Han, E.H.; Xu, L. Mechanical and corrosion properties in 3.5% NaCl solution of cold sprayed Al-based coatings. *Surf. Coat. Technol.* **2020**, *385*, 12537. [[CrossRef](#)]
37. Ma, J.; Wen, J.; Li, Q.; Zhang, Q. Electrochemical polarization and corrosion behavior of Al-Zn-In based alloy in acidity and alkalinity solutions. *Int. J. Hydrog. Energy* **2013**, *38*, 14896–14902. [[CrossRef](#)]
38. Mohammed, A.A. A newly synthesized glycine derivative to control uniform and pitting corrosion processes of Al induced by SCN-anions-Chemical, electrochemical and morphological studies. *Corros. Sci.* **2010**, *52*, 3243–3257.
39. Kumar, S.; Kumar, M.; Jindal, N. Overview of cold spray coating application comparisons: A critical review. *World J. Eng.* **2020**, *17*, 27–51. [[CrossRef](#)]
40. Pathak, S.; Saha, G. Development of Sustainable Cold Spray Coatings and 3D Additive Manufacturing Components for Repair/Manufacturing Applications: A Critical Review. *Coatings* **2017**, *7*, 122. [[CrossRef](#)]
41. Gadow, R.; Killinger, A.; Stiegler, N. Hydroxyapatite coatings for biomedical applications deposited by different thermal spray techniques. *Surf. Coat. Technol.* **2010**, *205*, 1157–1164. [[CrossRef](#)]
42. Zou, Y.; Qiu, Z.; Huang, C.; Zeng, D.; Lupoi, R.; Zhang, N.; Yin, S. Microstructure and tribological properties of Al<sub>2</sub>O<sub>3</sub> reinforced FeCoNiCrMn high entropy alloy composite coatings by cold spray. *Surf. Coat. Technol.* **2022**, *434*, 128205. [[CrossRef](#)]
43. Available online: <https://jteg.ncms.org/wp-content/uploads/2019/09/02-Aaron-JTEG-CS-4-28-2020.pdf> (accessed on 14 September 2022).
44. Che, H.; Liberati, A.C.; Chu, X.; Chein, M.; Nobari, A.; Vo, P.; Yue, S. Metallization of polymers by cold spraying with low melting point powders. *Surf. Coat. Technol.* **2021**, *418*, 127229. [[CrossRef](#)]
45. Che, H.; Phuong, V.; Stephen, Y. Investigation of cold spray on polymers by single particle impact experiments. *J. Therm. Spray Technol.* **2019**, *28*, 135–143. [[CrossRef](#)]
46. Che, H.; Chu, X.; Vo, P.; Yue, S. Metallization of various polymers by cold spray. *J. Therm. Spray Technol.* **2018**, *27*, 169–178. [[CrossRef](#)]
47. Chen, M.; Che, H.; Yue, S. Exploring surface preparation for cold spraying on polymers. *Surf. Coat. Technol.* **2022**, *450*, 128993. [[CrossRef](#)]

**Disclaimer/Publisher’s Note:** The statements, opinions and data contained in all publications are solely those of the individual author(s) and contributor(s) and not of MDPI and/or the editor(s). MDPI and/or the editor(s) disclaim responsibility for any injury to people or property resulting from any ideas, methods, instructions or products referred to in the content.